MASARYKOVA UNIVERZITA
PŘÍRODOVĚDECKÁ FAKULTA
ÚSTAV TEORETICKÉ FYZIKY A ASTROFYZIKY

Bakalářská práce

BRNO 2026 SIMONA HÁNOVÁ

MASARYKOVA
UNIVERZITA
PŘÍRODOVĚDECKÁ FAKULTA
ÚSTAV TEORETICKÉ FYZIKY A ASTROFYZIKY

Proměnné hvězdy v kulové hvězdokupě NGC 4833

Bakalářská práce

Simona Hánová

Vedoucí práce: Mgr. Marek Skarka, Ph.D. **Brno 2026**

Bibliografický záznam

Autor:	Simona Hánová Přírodovědecká fakulta, Masarykova univerzita Ústav teoretické fyziky a astrofyziky
Název práce:	Proměnné hvězdy v kulové hvězdokupě NGC 4833
Studijní program:	Fyzika
Studijní obor:	Astrofyzika
Vedoucí práce:	Mgr. Marek Skarka, Ph.D.
Akademický rok:	2025/2026
Počet stran:	vii + 35
Klíčová slova:	Proměnná hvězda; Kulová hvězdokupa; NGC 4833; Fotometrie

Bibliographic Entry

Author:	Simona Hánová Faculty of Science, Masaryk University Department of Theoretical Physics and Astrophysics
Title of Thesis:	Variable stars in globular cluster NGC 4833
Degree Programme:	Physics
Field of Study:	Astrophysics
Supervisor:	Mgr. Marek Skarka, Ph.D.
Academic Year:	2025/2026
Number of Pages:	vii + 35
Keywords:	Variable star; Globular cluster; NGC4833; Photometry

Abstrakt

Tato bakalářská práce se zabývá identifikací proměnných hvězd v kulové hvězdokupě NGC 4833. Fotometrická data získaná pomocí 1.54 m dalekohledu na observatoři La Silla v Chile byla analyzována pomocí programu `ISIS`, založeného na metodě odečítání snímků, a profilové fotometrie. Analyzovaný soubor dat obsahoval celkem 343 snímků v *R* filtru pořízených během 11 pozorovacích nocí. V pozorovaném poli bylo identifikováno celkem 23 kandidátů na proměnné hvězdy. Pro všechny detekované objekty byly sestrojeny světelné křivky a byly odhadnuty jejich periody proměnnosti. Na základě tvaru světelných křivek a odvozených period byla navržena předběžná klasifikace detekovaných proměnných hvězd. Většina identifikovaných objektů byla klasifikována jako kandidáti na pulzující hvězdy typu RR Lyrae. Dále byli identifikováni dva kandidáti na pulzující hvězdy typu SX Phoenicis a několik možných zákrytových dvojhvězd nebo rotačních proměnných hvězd. U některých objektů zůstává klasifikace nejistá z důvodu omezeného časového pokrytí pozorování a přítomnosti frekvenčních aliasů. Detekované proměné hvězdy byly také porovnány s kandidáty na chemicky pekuliární hvězdy poblikované v literatuře, avšak u těchto objektů nebyla detekována žádná zjevná proměnnost.

Abstract

This thesis investigates the identification of variable stars in the globular cluster NGC 4833. Photometric data obtained from the 1.54 m telescope at La Silla observatory in Chile were analyzed using the `ISIS` image subtraction software and profile photometry. The analyzed dataset consisted of 343 *R*-band frames obtained during 11 observing nights. A total of 23 candidate variable stars were identified in the observed field. Light curves were constructed for all detected objects and their variability periods were estimated. Based on the shapes of the light curves and the derived periods, the classifications of the detected variable stars were proposed. Most of the identified objects were classified as RR Lyrae candidates. In addition, two candidates for SX Phoenicis stars and several possible eclipsing binaries or rotational variables were identified. For some objects, the preliminary classification remains uncertain due to limited temporal sampling and the presence of alias frequencies. The detected variable stars were also compared with chemically peculiar star candidates reported in the literature. However, no clear variability was detected for these objects.

MUNI
SCI

MASARYKOVA UNIVERZITA
PŘÍRODOVĚDECKÁ FAKULTA
KOTLÁŘSKÁ 2, 611 37 BRNO
IČ: 00216224
DIČ: CZ00216224

ZADÁNÍ BAKALÁŘSKÉ PRÁCE

Akademický rok: 2025/2026

Ústav:	Ústav teoretické fyziky a astrofyziky
Studentka:	Simona Hánová
Program:	Fyzika
Specializace:	Astrofyzika

Ředitel *ústavu* PřF MU Vám ve smyslu Studijního a zkušebního řádu MU určuje bakalářskou práci s názvem:

Název práce:	Proměnné hvězdy v kulové hvězdokupě NGC 4833
Název práce anglicky:	Variable stars in globular cluster NGC 4833
Jazyk práce:	angličtina

Oficiální zadání:
Kulové hvězdokupy obsahují velké množství proměnných hvězd, které pomáhají určit jejich základní charakteristiky jako vzdálenost, věk a chemické složení. NGC 4833 byla měřena během více než dvaceti nocí s pomocí 1.54m dalekohledu na observatoři La Silla. Cílem práce bude s pomocí metody odčítání snímků identifikovat proměnné hvězdy, získat jejich světelné křivky a klasifikovat je. Speciální pozornost bude věnována (ne)detekci proměnnosti u kandidátů na magnetické chemicky pekuliární hvězdy identifikované v této hvězdokupě.

Literatura:
NEUMANNOVÁ, Kateřina. *Hvězdná proměnnost v kulových hvězdokupách*. Edited by Marek Skarka. ???

SKARKA, Marek a Zbyněk HENZL. Periodic variable A-F spectral type stars in the southern TESS continuous viewing zone: I. Identification and classification. *Astronomy and Astrophysics*. EDP Sciences, 2024, roč. 688, August 2024, s. 1-10. ISSN 0004-6361. Dostupné z: https://doi.org/10.1051/0004-6361/202450711.

MIKULÁŠEK, Zdeněk a Miloslav ZEJDA. *Proměnné hvězdy*. ÚTFA PřF MU. Brno, 2009.

Vedoucí práce:	Mgr. Marek Skarka, Ph.D.
Datum zadání práce:	29. 10. 2025
V Brně dne:	11. 5. 2026

Zadání bylo schváleno prostřednictvím IS MU.

Simona Hánová, 13. 11. 2025
Mgr. Marek Skarka, Ph.D., 30. 10. 2025
RNDr. Luboš Poláček, 11. 12. 2025

Poděkování

V prvom rade by som chcela poďakovať vedúcemu mojej bakalárskej práce Mgr. Marekovi Skarkovi, Phd. za čas, ochotu a cenné rady pri vedení mojej práce. Ďalej by som chcela poďakovať Mgr. Filipovi Hrochovi, Phd. za odborné rady, a Mgr. Magdalene Špokovej za pomoc pri spracovaní dát. Moje poďakovanie patrí aj pozorovateľom, ktorí získali pozorovacie dáta použité v tejto práci. Na záver by som chcela poďakovať mojej rodine a priateľom za pomoc a podporu počas celého štúdia.

Prohlášení

Prohlašuji, že jsem svoji bakalářskou práci vypracovala samostatně pod vedením vedoucího práce s využitím informačních zdrojů, které jsou v práci citovány.

Brno 13. května 2026 .....

Simona Hánová

Contents

Introduction

A study of variable stars is a fundamental area of stellar astrophysics. The changing brightness of stars provides direct insight into stellar structure, evolution and physical properties that cannot be obtained from stationary objects alone. The analysis of their light curves allows astronomers to determine stellar parameters such as mass, radius, temperature and internal structure. In addition, certain types of variable stars, such as RR Lyrae and Cepheids, serve as standard candles and are essential tools for determining distances on both galactic and extragalactic scales. For this reason, study of variable stars remains an important topic in modern astrophysical research.

Globular clusters represent an ideal environment for the study of variable stars. These systems contain large numbers of stars located at approximately the same distance from the observer, making it possible to compare their properties without the uncertainty introduced by distance variations. Many globular clusters host a significant population of variable stars, which are commonly used to determine cluster properties such as ages, distance and metallicities. These properties contribute to a better understanding of the structure, dynamical evolution and formation history of galaxies.

The main aim of this thesis is to analyze variable stars in the globular cluster NGC 4833. This globular cluster, located in the Milky Way halo, has not been studied as extensively as some other globular clusters, which makes it a suitable target for further analysis. The work includes the detection of variability, the construction and analysis of light curves and the classification of individual variable stars according to their variability type. Investigating variable stars in NGC 4833 can contribute to a better understanding of its physical properties. To achieve these goals, photometric methods suitable for crowded stellar fields are employed. In particular, image subtraction and profile photometry are used for obtaining brightness measurements from observational data.

This thesis is organized as follows. Chapter 1 provides a complex overview of variable stars, including the physical mechanisms underlying their variability and their classification. Chapter 2 focuses on the properties of globular clusters and their connection to variable stars. Chapter 3 presents photometric methods used for the identification of variable stars in crowded stellar fields. Chapter 4 describes observational data and the data reduction process. Chapter 5 presents the analysis of light curves and the classification of variable stars in NGC 4833. Finally, the results are discussed and summarized in the conclusion.

Chapter 1

Variable stars

1.1 Definition

Variable stars are stars whose brightness changes in time as observed from the Earth. Some of the variable stars exhibit only subtle variations, in the order of fractions of magnitudes, while others undergo abrupt and dramatic changes of several magnitudes. These variations may be periodic, semi-regular or irregular. They arise from a variety of physical processes, which form the basis for the classification of variable stars into multiple categories. The theoretical background presented in this chapter is primarily based on Mikulášek and Zejda (2013), unless stated otherwise.

1.2 Classification of variable stars

Variable stars can generally be divided into two main groups according to the origin of their variability. The first category consists of extrinsic variable stars. The light output of extrinsic variable stars does not change; instead, their observed brightness is affected by external factors such as eclipses by an orbiting companion or surrounding material that blocks or modulates the emitted light. In contrast, intrinsic variable stars undergo real changes in their physical properties, leading to variations in their luminosity. These processes include pulsations, flares and explosive outbursts (Bognár and Sódor 2025).

1.3 Extrinsic variable stars

1.3.1 Rotating variable stars

The brightness variation may arise from stellar rotation. Rapidly rotating stars have an aspherical shape with higher temperatures at the poles and lower temperatures near the equator. To observe a change in brightness of an aspherical star, precession of the star's rotating axis is necessary. Precession will cause axial asymmetry of the star and therefore variation in brightness with the stellar rotation.

Variability can also result from surface inhomogeneities such as starspots, which can be divided into two main categories. Photometric spots are characterized by a different

effective temperature compared to their surroundings. The most common are spots with lower effective temperature, therefore, are darker than the rest of the star's surface. They are caused by magnetic fields, which suppress the convection and, as a result, create a cooler spot. Bright spots with higher temperatures may also form, often due to accretion from a companion star or as a consequence of the reflection effect in close binary systems (Bognár and Sódor 2025). Chemical spots, on the other hand, have the same effective temperature but a different chemical composition from the rest of the star's surface.

The rotation is closely related to stellar activity and age. The magnetic field responsible for starspot formation is generated by a dynamo mechanism driven by the star's rotation. As stars age, they lose angular momentum, leading to slower rotation, reduced activity and fewer surface spots. Rotating variable stars can be further divided into subcategories with more specific properties.

Solar-type stars are main-sequence stars of spectral type G and K. These stars exhibit two types of variability: short-term variations caused by the rotation and movement of active regions across the stellar disk and long-term variations, which are analogous to the sun's eleven-year cycle. In addition, they may also exhibit solar-like oscillations.

FK Comae Berenices stars are giants of spectral type G and K that rotate very rapidly. This rapid rotation results in an ellipsoidal shape and high activity. The explanation for extremely fast rotation is not fully understood, but the most widely accepted theory proposes that FK Com stars form through the merger of a close binary system. The periods of their light variations correspond to the rotational periods of the stars and are typically on the order of several days. The amplitudes of the brightness variations can reach several tenths of a magnitude.

RS Canum Venaticorum stars exhibit multiple types of variability. They are part of a binary system that produces periodic brightness variation due to orbital motion. In addition, surface spots create semi-periodic or irregular changes in a star's brightness. This spot-induced variations typically have amplitudes up to 0.2 mag and occur on timescales ranging from days to years. The resulting light curve, presented in Fig. 1.1, is a combination of eclipses modified by a distortion wave caused by spots.

BY Draconis are magnetically active main-sequence stars of spectral types K and M. They may occur in binary systems or as single stars. They typically exhibit low-amplitude variability and strong chromospheric emission (Chahal et al. 2022). The periods of light variations are consistent with the rotational periods, ranging from a fraction of a day to several days.

Chemically peculiar stars are main-sequence stars with unusual abundances of particular chemical elements in their atmospheres. Their spectra show abnormally strong or weak spectral lines of certain elements. These stars often rotate slowly, and some possess magnetic fields that can be detected through polarization measurements of spectral lines (Schöller and Hubrig 2015). Elements on CP stars with a magnetic field concentrate in specific regions and create chemical spots.

Pulsars are rapidly rotating, highly magnetized neutron stars. They have periods ranging from 1.4 ms to 8.5 s. Pulsars produce beams of radiation that can be observed as periodic pulses. The different energy sources that power the pulsars' emission divide pulsars into different categories. The rotational energy of a neutron star can be used to power the emission, which can be observed as an increasing spin period of pulsars. Another

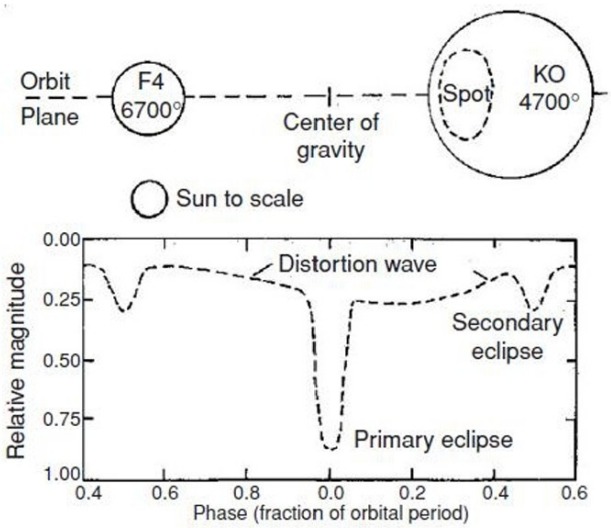

Figure 1.1: Schematic light curve of RS CVn variable with combination of distortion wave and eclipses (Percy 2007b).

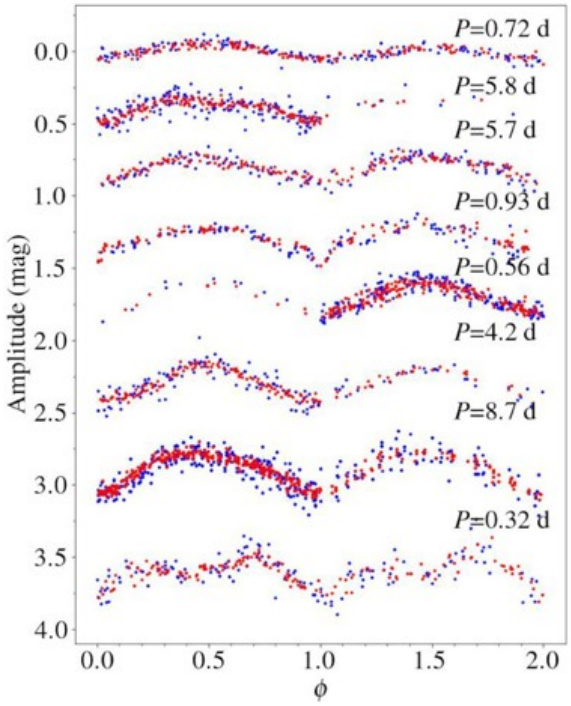

Figure 1.2: Example light curves of type BY Draconis variables (Chahal et al. 2022).

source of energy can be accretion of mass from a companion star, which is the case of X-ray binaries. The magnetic energy is the source of energy for pulsars with powerful magnetic fields called magnetars (Mereghetti 2013).

1.3.2 Eclipsing binaries

In a binary system, brightness variations occur due to eclipses and interaction between the two components. If the plane of orbital motion of the binary system is oriented favorably to the observer, one star passes periodically in front of the other, causing eclipses. The probability of observing eclipses increases for systems with smaller orbit relatively to the size of stars.

Based on the shape of their light curves, binary systems can be divided into the following three phenomenological classes.

Algol type (EA) systems exhibit light curves with deep and narrow primary minima and typically shallower but also narrow secondary minima. This decrease in brightness is caused by mutual eclipses of the two components. Outside of eclipses, the brightness of the systems remains constant. Algolid of type I has primary and secondary minima of similar depth and not deeper than 0.8 mag. Algolid of type II is characterized by deep primary minima, but secondary minima are not very distinct or are not present at all.

β Lyrae type (EB) systems show continuous variation in brightness, even outside eclipses. The primary and secondary minima have different depths. These systems generally have periods longer than one day.

W Ursae Majoris type (EW) systems display continuous brightness variations, with no clearly defined beginning or end of eclipses. The primary and secondary minima have nearly equal depths. These systems typically have short periods of less than one day.

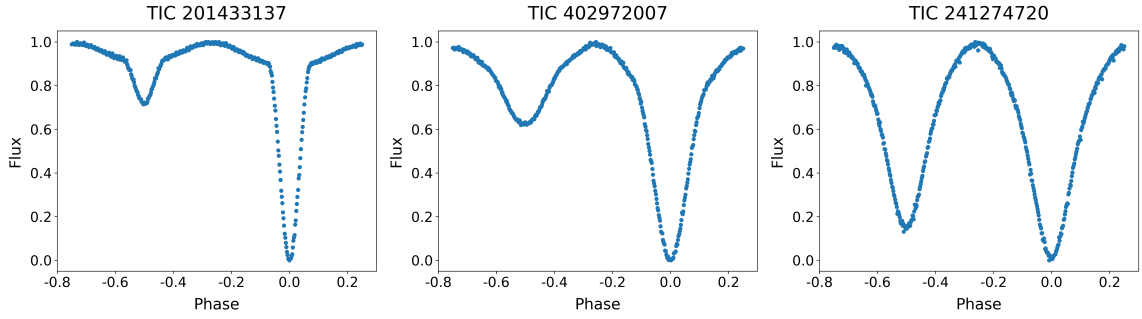

Figure 1.3: Light curves of eclipsing binaries: Algol type (left), β Lyrae type (middle), W Ursae Majoris type (right) (Liu et al. 2026).

Gravitational potential can also be used for the classification of binary systems (Kopal 1955). In such systems, the gravitational influence of both stars, together with the rotation of the system, creates surfaces of equal potential known as Roche equipotentials. The shape of the Roche equipotentials depends mainly on the mass ratio of the components and the distance between them. Of particular importance is the critical equipotential passing through the Lagrangian point L_1, where matter can flow from one component to another.

The extent to which the stars fill their Roche limit, or the largest closed equipotential capable of containing the masses of both stars, forms the basis for the classification of close binary systems.

Detached systems: The volumes of both components are smaller than the limit Roche equipotential. For this type of systems orbital period remains constant.

Semi-detached systems: The secondary component's volume is exactly the same as

its Roche limit, unlike the primary component, whose volume is smaller than its Roche limit.

Contact systems: Both components fill exactly their limit Roche equipotentials. This means that components are probably in contact at the location of the Lagrangian point L_1. In contrast to detached systems, the orbital periods of semi-detached and contact systems can change abruptly.

1.4 Intrinsic variable stars

1.4.1 Pulsating stars

Pulsating stars vary in brightness due to periodic changes in the shape and size of their surface. In case of radial pulsation, the radius of the star changes, which affects its temperature. As the radius increases, the surface temperature decreases and vice versa. Stars can be approximated as spheres, therefore radial pulsation represents the simplest form of pulsation. Radial pulsation corresponds to spherically symmetric expansion and contraction of the stellar surface and may occur in different pulsation modes. The simplest mode is called the fundamental mode, when all parts of a star expand and contract together. The next mode, which is more complicated than fundamental, is called the first overtone. In this mode, there is a nodal sphere in the star. The material that is part of the nodal sphere remains at rest, while the part of the star that is outside this sphere is expanding, and the part inside the sphere is contracting and vice versa. In the next mode, the second overtone, there are two nodal spheres where material remains at rest (Percy 2007a).

Stars are in hydrostatic balance, meaning all the forces acting on each element of the star compensate each other. This balance is stable, which means that in case of a disturbance, the forces try to bring the system back to equilibrium. Due to inertia, the star trying to reach the equilibrium surpasses this state and continues in its motion. This process creates oscillations around the equilibrium. Period P of pulsations is a function of the mean density of a star $\bar{\rho}$ as follows:

$$P \sim \frac{1}{\sqrt{G\bar{\rho}}} \tag{1.1}$$

where G denotes the gravitational constant. Eq. 1.1 shows that bigger stars with lower density have longer pulsation periods, which extend to hundreds of days. On the other hand, smaller, more compact stars, for example, δ Scuti stars, can have periods shorter than one hour.

Another case of pulsations are non-radial pulsations, which are harder to describe as they are not spherically symmetric. This type of pulsation is often characterized by the simultaneous presence of multiple pulsation modes. They usually exhibit lower amplitudes and more complex frequency spectra. In contrast, radial pulsations are usually dominated by one or a few modes and frequently exhibit larger amplitudes (Eggen 2008). Non-radial pulsations are commonly observed in δ Scuti and SX Phoenicis stars, while high-amplitude radial pulsations are characteristic of RR Lyrae stars and Cepheids.

Cepheids are radial pulsators with characteristic periods ranging from 1 to 100 days and high-amplitude light variations. Cepheids can be divided into two subcategories. Classical

Cepheids or type I Cepheids are young supergiants. They evolved from the main-sequence and have masses from 4 $M_\odot$ to 9 $M_\odot$. Type II Cepheids are old low-mass stars, with their mass in the range $0.5 - 0.6\ M_\odot$. They have a burning helium in a shell around their core, a highly inflated atmosphere and therefore high luminosity (Bognár and Sódor 2025). Cepheids are also called standard candles because of their well-defined period-luminosity relation. Cepheids with longer periods are more luminous. Their brightness and high amplitude light variations make Cepheids important distance indicators on the galactic and even extragalactic scales.

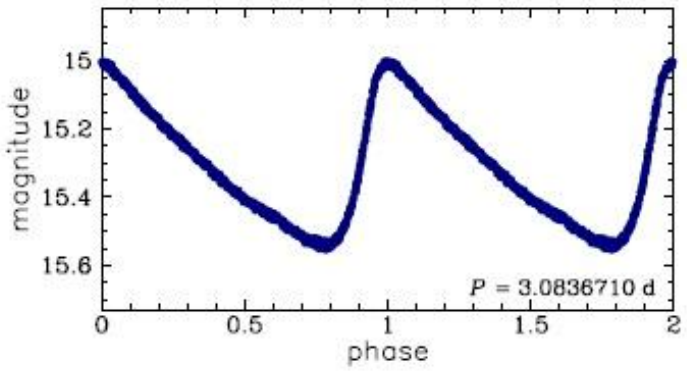

Figure 1.4: Light curve of classical Cepheid (OGLE Project 2011a).

RR Lyrae stars are large-amplitude pulsators with mainly fundamental and first overtone radial modes. However, additional non-radial pulsations have also been recently observed in their light variations. They are old giants and subgiants with typical masses between 0.5 and 0.8 $M_\odot$ and spectral classes from A to F. Owing to their old age, RR Lyrae stars may also be found in globular clusters. Periods of pulsation are in the interval from 0.2 to 1.2 days with amplitude variation from 0.2 to 2.5 mag. In the case of RR Lyrae stars, it is also possible to determine some physical properties of a star, such as metallicity, by analyzing the light curves (Fig. 1.5). In many RR Lyrae stars, periodic modulations of shape and period of the light curves have been observed. These modulations are known as the Blazhko effect and are the main open question in RR Lyrae research (Bognár and Sódor 2025).

Another type of pulsating variables are δ **Scuti** stars, which are stars of spectral types of A and F with radial and non-radial pulsation. They are in the main-sequence or immediate post main-sequence stage of evolution. The pulsations in δ Scuti stars are excited by the opacity mechanism in zone He II (Bognár and Sódor 2025). Observed amplitude variations are typically from 0.003 mag to 0.9 mag, with short periods of 0.01-0.2 days. Stars with higher amplitude variation are called high amplitude delta Scuti stars (HADS). The shape of the light curve and amplitude usually change with time. This is caused by the fact that these stars have many pulsation periods and different pulsating modes. Subcategory of stars of δ Scuti type are SX Phoenicis. Compared to classical δ Scuti stars, they exhibit higher amplitude variations with periods ranging from 0.03 to 0.08 days and are often found in the blue stragglers region of globular clusters (Sect. 2.4).

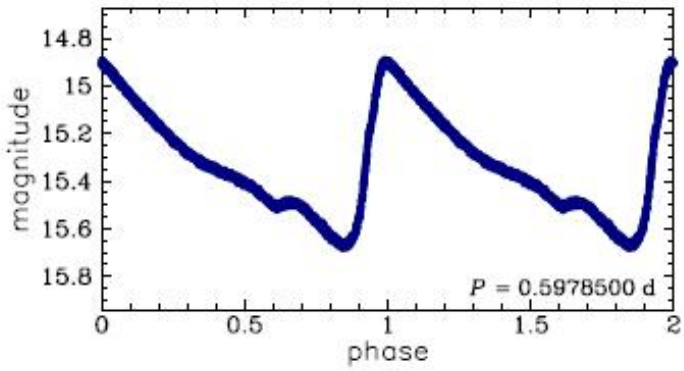

Figure 1.5: Light curve of RR Lyrae (OGLE Project 2011b).

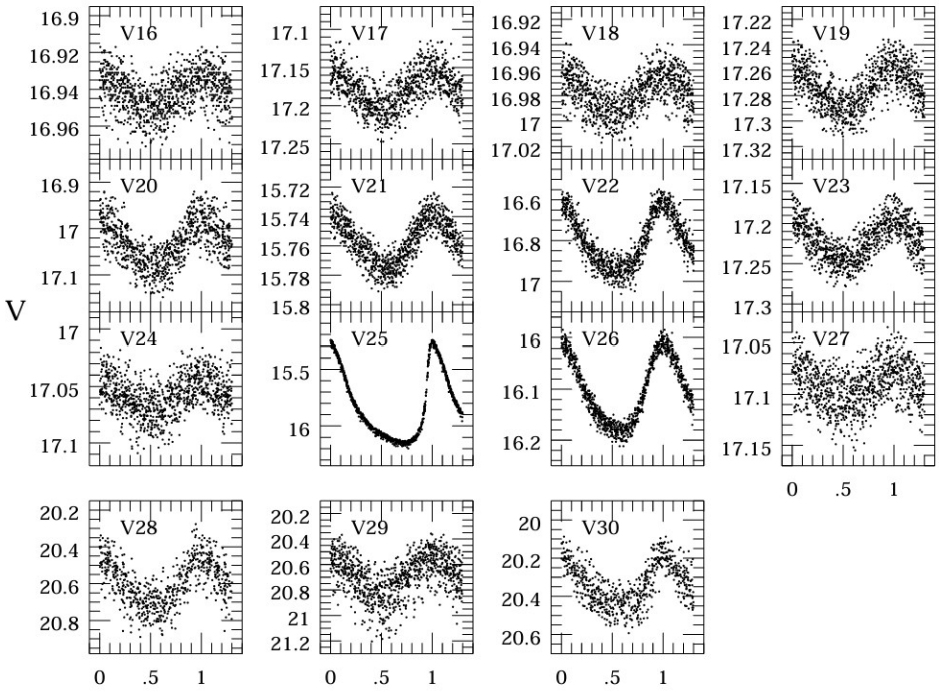

Figure 1.6: Light curve of SX Phe variables in globular cluster M55 (Pych et al. 2001).

1.4.2 Cataclysmic stars

Novae form from binary systems that consist of a white dwarf and a companion star filling its Roche lobe. Material transferred from the companion accumulates on the surface of a withe dwarf. This process heats the white dwarf and the layer of transferred material. When sufficient temperature and pressure are reached, unstable nuclear burning occurs, producing a sudden increase in brightness of up to 10-12 magnitudes. After an explosion, a white dwarf remains intact, and the process may repeat in the future (Chomiuk, Metzger, and Shen 2021).

Supernovae are variable stars that are not periodic and their variability is nonrecurring. A star can explode as a supernova only once. After the explosion, the star changes

dramatically. Either it ceases to exist, or it becomes a neutron star or a black hole. Classification of supernovas is based on the presence of chemical elements in their spectra.

Type I supernovae are characterized by the absence of lines of Hydrogen, while type II supernovae contain these lines in their spectrum. We can further divide type I supernovas into three other subcategories, which are type Ia, Ib and Ic. These can be distinguished by the presence of the Si II line and He lines. Type Ia supernovae generally originate from binary systems containing a white dwarf accreting matter from a companion star. When the white dwarf approaches critical mass, termonuclear reactions ignite through the star, leading to its complete disruption. Type II supernovae are the result of the evolution of massive stars. They are produced by the core collapse of these stars after nuclear fuel in their core is exhausted. The resulting explosion ejects the outer layers of the star into the surrounding space.

Chapter 2

Globular clusters

2.1 Definition and basic properties

Globular clusters are gravitationally bound objects. They are composed of tens of thousands to millions of stars that are relatively close to one another. Their concentration increases towards the center of the cluster. They typically exhibit a symmetrical spherical shape, as shown in Fig. 2.1 of the brightest globular cluster ω Centauri (NGC 5139). However, there are exceptions to this rule, as some globular clusters display an elliptical shape, but such cases are relatively rare. Typical values for the radius of a globular cluster are on the order of 3 to 5 pc (Gratton et al. 2019). Moreover, they are among the oldest objects in the universe, with ages ranging from 11 to 12.5 Gyr (VandenBerg et al. 2013).

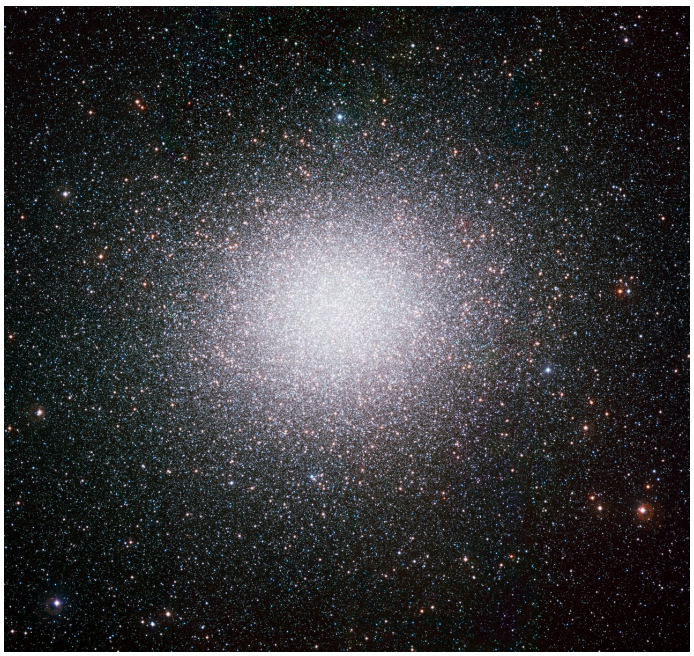

Figure 2.1: Image of ω Centauri (European Southern Observatory (ESO) 2008).

2.2 Classification of globular clusters

Globular clusters in the Milky Way can be divided into two main categories. These groups differ in their location in the Galaxy, metallicity and origin. Clusters located in the galactic halo are often referred to as blue globular clusters. They have low metallicity and probably previously belonged to the satellite galaxy. They may have been accreted during mergers with such a galaxy or captured through tidal interactions. In contrast, red globular clusters are found in the Galactic disk or bulge. They are more concentrated towards the Galactic center and tend to rotate with it. These globular clusters are relatively younger and metal-rich. They are believed to have formed in-situ within the Galaxy (Arkelyan and Pilipenko 2022).

2.3 Comparison with open clusters

There are several important differences between open and globular clusters. Open clusters generally have irregular shapes, while globular clusters are approximately spherically symmetric (Fernie, Chaisson, and Hogg-Priestly 2025). The number of stars in open clusters is typically lower, from tens to thousands. In the case of globular clusters, the number of stars can reach up to millions. Furthermore, stars in globular clusters are strongly gravitationally bound, whereas open clusters can gradually disperse into individual stars over time. As a consequence, globular clusters are much older structures than open clusters, as their strong gravitational binding allows them to remain intact over long timescales. The stellar population of clusters also differs. Globular clusters consist predominantly of population II stars, which are older and metal-poor, while open clusters contain younger population I stars. Open clusters are primarily located in the Galactic disk, whereas most of the globular clusters are found in the Galactic halo or bulge (Gratton et al. 2019).

2.4 (Variable) stars in globular clusters

The analysis of stars in globular clusters allows us to determine the properties of these systems. Since the stars within the globular cluster can be considered to lie at approximately the same distance from the Earth. The effect of distance on their observed brightness is practically the same for all cluster members. This represents a significant advantage, as differences in luminosity between stars can be studied independently of distance effects.

For this purpose, the Hertzsprung-Russell (HR) diagram is commonly used. This diagram represents the relationship between the color index or spectral type of a star and its magnitude. HR diagrams of globular clusters show a major grouping of stars along the lower main sequence. From this sequence extends the giant branch, containing more luminous stars, curving to the upper right part of the diagram. Horizontal branch stars are located roughly halfway up the giant branch and extend horizontally toward the left part of the diagram (Fernie, Chaisson, and Hogg-Priestly 2025).

The point at which the stars begin to leave the main sequence and evolve toward the giant branch is known as the turnoff point, and it is commonly used to estimate the age of the cluster. In younger clusters, the formation of the turnoff point begins with the more

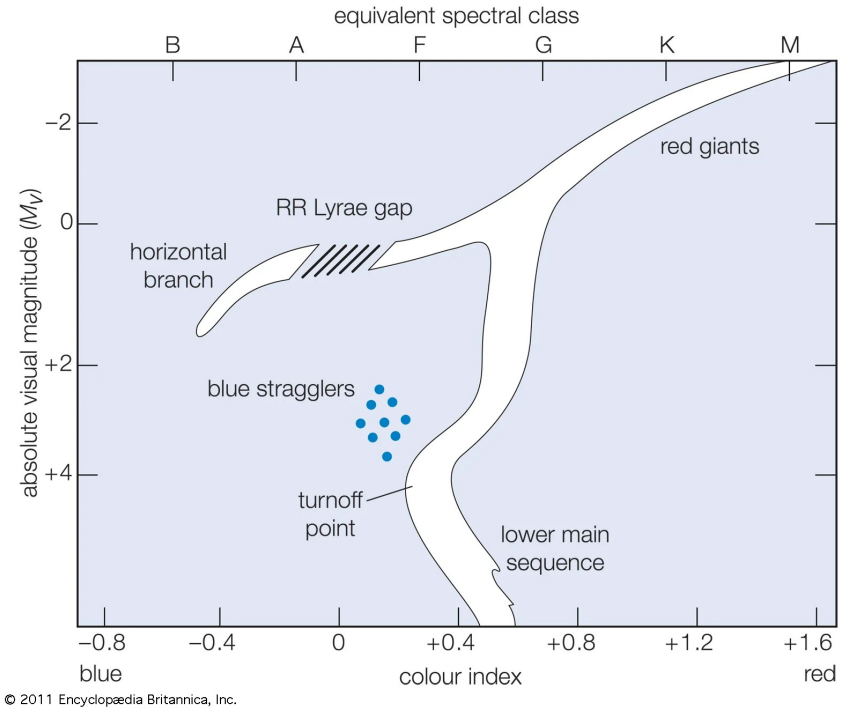

Figure 2.2: HR diagram of a globular cluster showing the main sequence, turn off point, blue stragglers, giant branch and horizontal branch (Fernie, Chaisson, and Hogg-Priestly 2025).

massive, hotter stars evolving off the main sequence. With increasing age of the globular cluster, the turnoff point moves to colder stars.

One feature of globular cluster HR diagrams remains an open question: the presence of stars known as blue stragglers. These stars are located near the main sequence, even though, based on their mass and temperature, they should already have evolved off the main-sequence, similarly to the majority of stars with comparable properties within the cluster. One possible explanation is that blue stragglers formed through the merger of two less massive stars. This turned them into more massive and apparently younger star located near the main sequence. However, this explanation does not account for all observed cases of blue stragglers (Fernie, Chaisson, and Hogg-Priestly 2025).

The study of variable stars in globular clusters also contributes to determining some of the cluster properties. The most common variable stars in globular clusters are RR Lyrae stars (described in Sect. 1.4.1). In Arellano Ferro and Prudil (2026), light curves of RR Lyrae variables are used to determine the distance and metallicities of 24 globular clusters located in the Galactic bulge. Additionally, Boyles et al. (2011) suggests a possible relation between the presence of pulsars (Sect. 1.3.1) and the metallicity of the cluster. Other types of variable stars found in globular clusters include Cepheids (Sect. 1.4.1), eclipsing binaries (Sect. 1.3.2), and others.

2.5 NGC 4833

NGC 4833 is one of the globular clusters located within the Milky Way at a distance of 6.6 kpc from Earth (Boyles et al. 2011). It is situated in the constellation Musca and is therefore visible only from the Southern Hemisphere. It is a metal-poor ([Fe/H] = -2.04) (E. Carretta et al. 2014) globular cluster that exhibits evidence of multiple stellar populations (Eugenio Carretta 2021). According to Forbes and Bridges (2010), the estimated age of NGC 4833 is 12.54 Gyr.

This globular cluster was discovered by Abbe Lacaille during his expedition to South Africa in 1751-1752. It was later observed and classified by James Dunlop and Sir John Herschel, who were able to resolve it into individual stars with the help of their instruments.

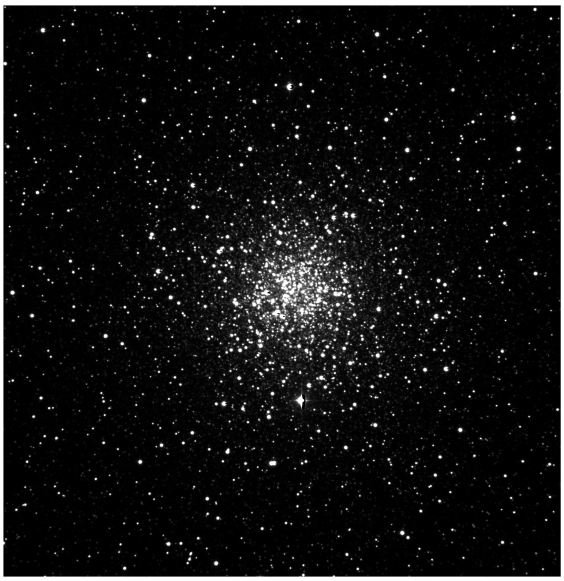

Figure 2.3: Image of globular cluster NGC 4833 obtained with the 1.54 m telescope at La Silla observatory.

This globular cluster has also been the subject of photometric studies. In Špoková et al. (2026), candidates for chemically peculiar stars were identified in a sample of Milky Way globular clusters, including NGC 4833, using multicolor photometry. The photometric measurements were obtained using profile photometry performed in the `IRAF` software package. The identification of the chemically peculiar stars is particularly relevant in the context of this thesis. One of the objectives of the analysis is to investigate whether any of the detected variable stars can be associated with these previously identified candidates for chemically peculiar stars. Such a connection could provide additional insight into the nature of the variability and physical properties of these objects.

Chapter 3

Photometry

3.1 Fundamental concepts

Light coming from a distant object can be interpreted as a stream of photons with different energies. For energy E and momentum p of photon we can write

$$E = h\,\nu, \qquad p = \frac{h}{\lambda}, \tag{3.1}$$

where $\nu = \frac{c}{\lambda}$ is frequency of the photon, λ denotes wavelength, $h = 6.626069 \cdot 10^{-34}$ Js is Plank's constant and $c = 2.99792458 \cdot 10^{8}$ ms^{-1} is the speed of light.

The luminosity L of a star is defined as the total amount of energy emitted over all wavelengths per unit time in all directions. In practice, however, only a fraction of the emitted energy can be detected. This fraction depends on the collecting area of the detector and its distance from the source. The energy received per unit area per unit time is called the flux F and is given as

$$F = \frac{L}{4\pi r^2}, \tag{3.2}$$

with r being the distance of the detector from the source.

The brightness of a star is commonly expressed using the quantity called magnitude m. It is linked to flux F by Pogson's equation (Pogson 1856)

$$m_1 - m_2 = -2.5 \log\left(\frac{F_1}{F_2}\right). \tag{3.3}$$

Magnitude differences can be used to compare either two different objects or the brightness of the same object observed at different times. In this equation, m_1 and m_2 represent the corresponding magnitudes, while F_2 and F_1 denote the measured fluxes.

Magnitude m defined in Eq. 3.3 is referred to as apparent magnitude. This quantity depends on the distance to the star. A star, that is intrinsically brighter than another star, can have a higher apparent magnitude (fainter) if it is located farther away from the Earth. For this reason, the absolute magnitude M is introduced. It is defined as the apparent magnitude a star would have if it were observed from a distance of 10 parsecs and is calculated as follows:

$$m - M = 5 \log(d) - 5. \tag{3.4}$$

This equation connects the apparent and absolute magnitude of a source with its distance d in parsecs. Expression $m - M$ is known as the distance modulus.

The star emits radiation across the entire electromagnetic spectrum. In photometry, however, observations are usually performed only within selected wavelength intervals defined by photometric filters. Measurements in different filters provide information about the spectral energy distribution (SED) of a star and allow the determination of its physical properties, such as temperature.

One of the most widely used systems of photometric filters is Johnson's photometric system (Johnson and Morgan 1953). It consists of three primary filters: U (300-420 nm, peak at 360 nm), B (360-560 nm, peak at 420 nm) and V (460-740 nm, peak at 535 nm). The Johnson's system was expanded with additional filters R (700 nm) and I (900 nm) (Kron and Smith 1951; Cousins 1976) and by infrared filters J (1250 nm), H (1650 nm) and K (2200 nm).

Between the measured object and the detector exists a medium that is not perfectly transparent. Radiation can be absorbed or dispersed by interstellar material or by molecules of air and water in Earth's atmosphere. As a result, the observed light source is attenuated. This effect is known as extinction.

Photometric measurements are typically represented by a light curve, which shows the variation of brightness as a function of time, usually in Julian Date. The analysis of light curves provides valuable information about stellar properties, including periods, amplitudes of variability, and possible mechanisms responsible for the observed brightness changes. The shape of the light curve can also be used for classification of variable stars, since different types of variability produce characteristic light-curve profiles Sect. (1).

An example of the obtained light curve in this work is shown in Fig. 3.1. The figure presents the brightness variations of one of the identified variable stars during the observing night with the largest number of acquired frames. The changes in brightness visible in the light curve indicate the variable nature of the object.

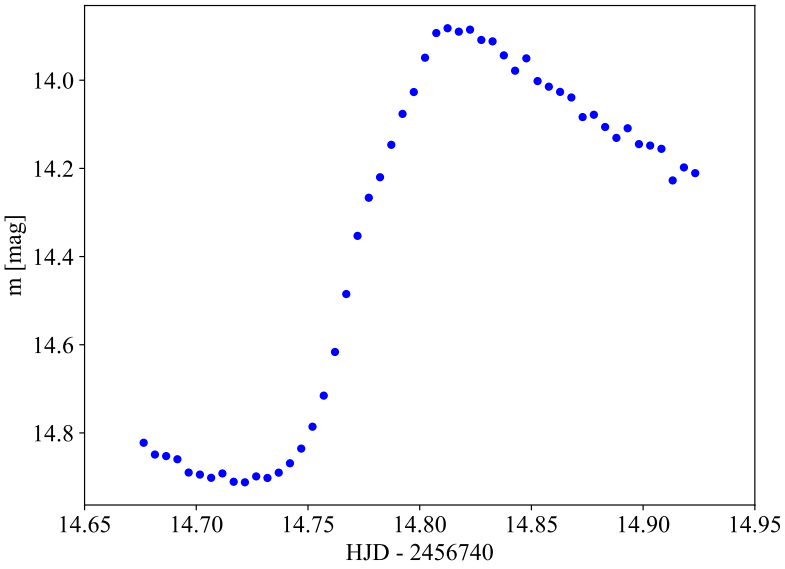

Figure 3.1: Example of light curve of one of the identified variable stars in NGC 4833.

3.2 Periodic variability

Variability of stellar brightness can be periodic, semi-periodic or irregular. In the case of periodic variable stars, the brightness changes repeat after a certain interval of time called the period P. Determination of the period is one of the fundamental tasks in the analysis of variable stars, since it provides important information about the physical nature of the observed object.

The period of variability can be determined using frequency analysis methods, most commonly based on the Fourier transformation. These methods search for dominant frequencies present in the light curve data. The period can then be determined from the corresponding dominant frequency f

$$P = \frac{1}{f}. \tag{3.5}$$

Once the period is determined, the observational data can be transformed into a phase-folded light curve. The phase ϕ is defined as

$$\phi = \text{frac}\left[\frac{t - M_0}{P}\right] \tag{3.6}$$

where t is the observation time, M_0 is a reference epoch and frac denotes the fractional part of the expression. The phase therefore takes values in the interval from 0 to 1.

This process, known as phase-folding, makes it possible to combine measurements from multiple cycles into a single representation of the variability. As a result, the characteristic shape of the light curve becomes more clearly visible, which facilitates the classification and analysis of variable stars.

An example of phase-folding is shown in Fig. 3.2. Figure 3.2a presents the original unphased light curve, where the periodic behavior is difficult to recognize. After applying the derived period, the measurements can be transformed into phase space, producing the phase-folded light curve shown in Fig. 3.2b. The periodic variability and characteristic shape of the light curve become significantly more visible after phase-folding.

3.3 Aperture photometry

In order to measure the brightness of an object, it is first necessary to determine the signal recorded on the detector and subsequently calibrate the measurement. Aperture photometry is the most widely used photometric method. It is based on isolating the measured object in order to determine the amount of light originating from that object.

Historically, this method was first implemented using photomultipliers. The observed object was placed within a physical aperture that blocked the rest of the field of view. In this configuration, only the light from the object entered the detector. However, the measured signal was contaminated by the background light. Therefore, an additional measurement of the background was required, and its contribution was subtracted from the object measurement to obtain the final flux (Janík 2021).

In the case of CCD detectors, the same principle is applied, but the apertures are defined digitally after the frames are acquired. This approach allows aperture photometry

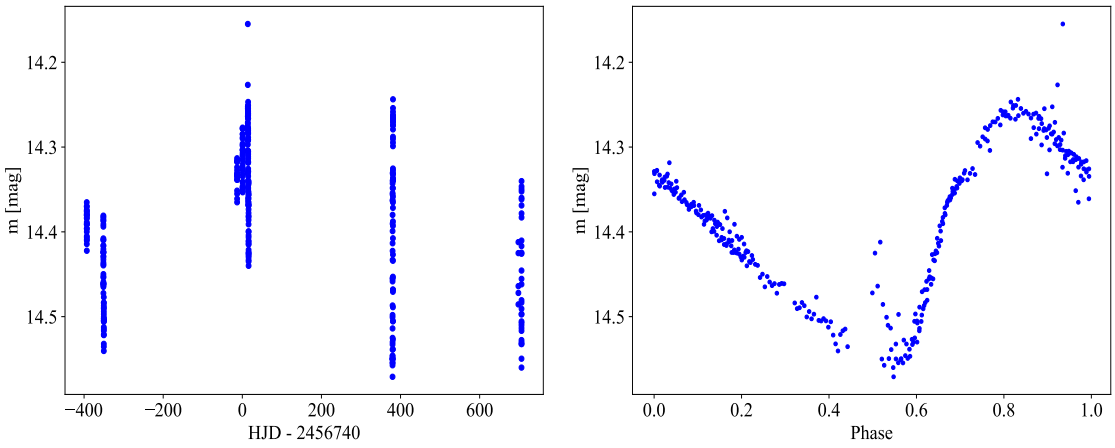

(a) Unphased light curve.

(b) Phase-folded light curve.

Figure 3.2: Example of phase-folding.

to be performed simultaneously for a large number of objects within a single frame, which represents a significant advantage compared to the photomultiplier-based observations.

The choice of an appropriate aperture size is crucial. If the aperture is too small, a fraction of the object's flux is lost. On the other hand, if the aperture is too large, additional noise from the background is included. This is illustrated in Fig. 3.3.

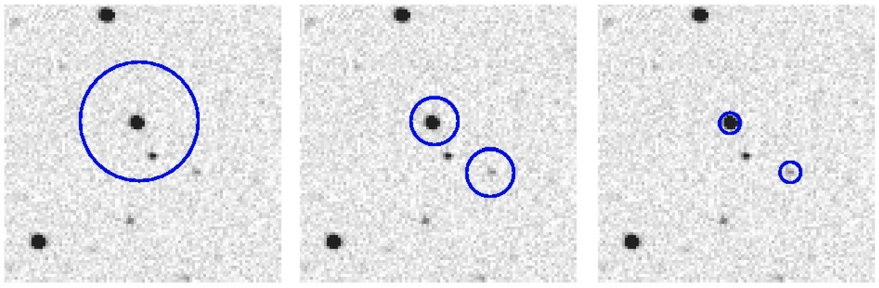

Figure 3.3: Example of different aperture sizes. The aperture in the left is too large, the one on the right is too small, and the middle aperture represents an optimal choice (Janík 2021).

The brightness of an object is defined as

$$m = C - 2.5 \log \frac{\sum_{i,j} w_{i,j} A_{i,j} - b}{t_{\text{exp}}} \tag{3.7}$$

where $A_{i,j}$ represents the recorded signal in the pixel at position (i, j), $w_{i,j}$ is a weight assigned to each pixel, the term b defines the contribution of the background, t_{exp} is exposure time, and constant C is used to transform instrumental magnitude to a standard photometric system.

3.4 Profile photometry

Profile photometry is another method suitable for crowded fields. This type of photometry is described in Stetson (1987) and is based on modeling the point spread function (PSF) to determine the magnitudes of stars in the frame.

The point spread function describes the two-dimensional brightness distribution produced by a luminous object such as a star. Its shape varies from frame to frame due to changes in observational conditions (temperature, seeing and other atmospheric conditions). Therefore, determining the PSF represents a challenging task for astronomers. In Stetson (1987), the author proposes a method for defining PSF that combines an analytic and empirical approach. The principle of this method is to start with a Gaussian function

$$F_0(n) = \frac{1}{\sqrt{\pi/2}} e^{-(n-n_0)^2/\sigma^2} \tag{3.8}$$

as the first-order approximation to the actual stellar profile. The residuals, which represent the difference between the model PSF (Gaussian) and the actual data, are used to correct the model function. This process is repeated until the corrections become negligible.

In practice, several stars are chosen whose observed profiles are fitted with the first-approximated function. These fitted profiles are added to the empirical PSF, which is built star by star. In the case of a crowded field, the majority of the stars are blended with nearby neighbors. This results in the model PSF not accurately representing the true PSF in the frame.

Nevertheless, the fitting of the first estimated PSF to the stars and their known neighbors in the frame is performed. Subtraction of the fitted profiles produces residuals, and the neighboring stars, which blend with the chosen stars, are no longer present in the subtracted frame. However, subtraction of the neighboring stars is not perfect, but they contaminate the profiles of the bright stars less than they did in the original frame.

After the subtraction of the neighbors, the chosen stars are once again added together to produce a new model PSF. This new function is again fitted to the stars and their neighbors in the original frame, and they are again subtracted. The fits are considerably better this time. After repeating this process the third time, there is almost no evidence of the systematic errors caused by the bright stars' neighbors.

Once the PSF is successfully determined, the magnitude m can be obtained by integrating it:

$$m = -2.5 \log \int_{x,y} F(n)\, \mathrm{d}x\mathrm{d}y + C \tag{3.9}$$

where $F(n)$ represents the PSF and constant C is used in transformation into standard photometric system.

3.5 Image subtraction

In crowded stellar fields, specialized techniques are required for the analysis of photometric data. One such method is image subtraction, described in Alard and Lupton (1998). It is based on detecting the variation in a star's brightness by subtracting images from a

reference frame. In practice, it combines elements of aperture and profile photometry to achieve accurate measurements in densely populated regions.

Selecting an optimal reference frame is essential for the proper functioning of this method. A reference frame with the best seeing is typically chosen to ensure optimal results. The remaining frames often differ slightly in orientation and center from the reference frame. Therefore, an astrometric transformation must be performed to align the coordinates of all frames with the reference frame. In Alard and Lupton (1998), 500 stars are selected on the reference frame and the other frame to determine the transformation using a two-dimensional polynomial. As a result, all frames are on the same coordinate system as the reference frame.

After coordinate alignment, it is necessary to match the seeing of the reference frame and the rest of the frames. A complication arises because the frames do not have the same point spread functions. Assuming that most stars on the frame do not exhibit large amplitude variations, a large number of the pixels in different frames would be very similar if the seeing were identical. Therefore, the kernel, which represents the transformation needed to match the PSF of the reference image and the rest of the frames, can be found by finding the least square solution of the following equation:

$$\mathrm{Ref}(x,y) \otimes \mathrm{Kernel}(u,v) = I(x,y) \tag{3.10}$$

where Ref is the reference frame and I is the frame we want to align with the reference. The symbol $\otimes$ stands for convolution.

Although this problem is formally nonlinear, it can be transformed into a linear least-squares problem. In Alard and Lupton (1998), the authors propose a solution by decomposing the kernel into basic functions. Thanks to the decomposition, the non-linear problem becomes a standard linear least squares problem. The decomposition of the kernel is described in the equation below:

$$\mathrm{Kernel}(u,v) = \sum_i a_i \times B_i(u,v) \tag{3.11}$$

The solution for the least squares gives the matrix equation for the coefficients a_i.

$$M\mathrm{a} = V \tag{3.12}$$

Matrix M represents scalar products of the vectors C_i and the vector V represents the scalar product of C_i with the I. Set of vectors C_i is defined as:

$$C_i(x,y) = I(x,y) \otimes B_i(x,y) \tag{3.13}$$

The solution to this problem is to find a suitable basis of functions to model the kernel. In Alard and Lupton (1998), a set of Gaussian functions is used, which are modified by multiplication with a polynomial. Consequently, the decomposition of the kernel has the following structure:

$$\mathrm{Kernel}(u,v) = \sum_n \sum_{d_n^x} \sum_{d_n^y} a_n \times e^{-(u^2+v^2)/2\sigma_n^2} u^{d_n^x} v^{d_n^y} \tag{3.14}$$

where $0 < d_n^x \leq D^n$, $0 < d_n^y + d_n^x \leq D^n$ and D^n is the degree of the polynomial relevant to the n$^{\text{th}}$ Gaussian function. In practice, it should be sufficient to use 3 Gaussian components with a polynomial degree between 2 and 6.

This method can also be extended to model the differential background variation. It is executed by modifying the equation (3.10).

$$\text{Ref}(x,y) \otimes \text{Kernel}(u,v) = I(x,y) + bg(x,y) \tag{3.15}$$

For $bg(x,y)$ it is used following polynomial expression:

$$bg(x,y) = \sum_i \sum_j a_i x^i y^j \tag{3.16}$$

with $0 < i \leq D^{bg}$, $0 < i + j \leq D^{bg}$, where D^{bg} is the degree of the polynomial which is used for modeling the differential background variation. The least square solution for the modified equation (3.15) will result in the matrix equation similar to the equation (3.12). The definition of matrix M and vector V stays the same, but it is necessary to augment the number of vectors C_i.

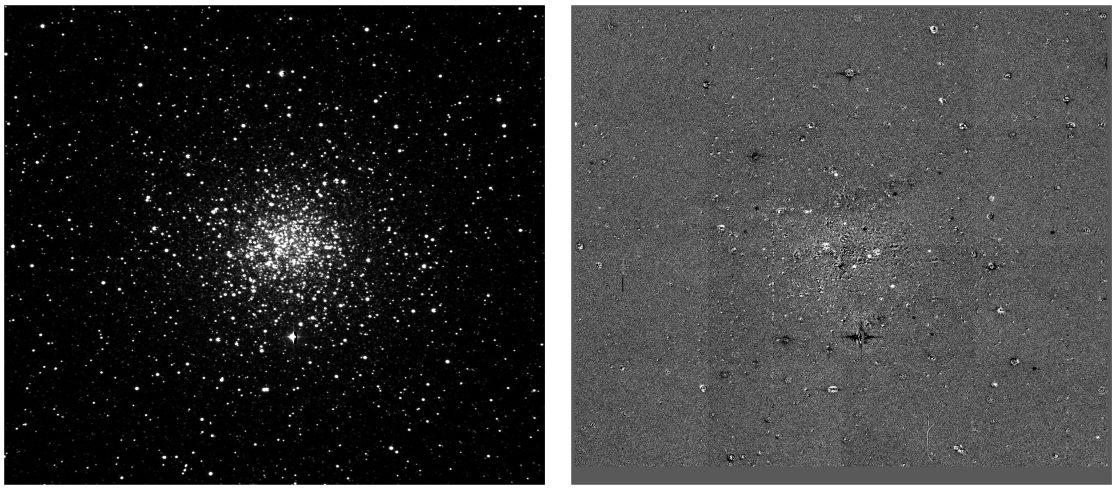

(a) Original frame. (b) Frame after subtraction.

Figure 3.4: Example of image subtraction.

Chapter 4

Observations and light curves

The observational data in this thesis were obtained with the Danish 1.54 m telescope at La Silla Observatory in Chile, equipped with the DFOSC CCD imager. The detector consists of a 2048×2048 CCD providing a field of view of 13.5×13.5 arcmin with a spatial resolution of 0.396 arcsec/px (Shafter et al. 2021). The full available data set consists of frames acquired in 32 nights. From this set, data from 11 nights with a sufficiently large number of high-quality frames were selected for further analysis. These nights are listed in Tab. 4.1.

date	frames	B	V	R	I
2013-2-22	99	25	25	25	24
2013-4-5	134	33	34	34	33
2013-4-6	92	23	23	23	23
2014-3-9	67	17	17	17	16
2014-3-23	127	32	32	32	31
2014-4-5	59	16	15	15	13
2014-4-6	204	51	51	51	51
2014-4-7	139	35	35	35	35
2015-4-6	144	36	36	36	36
2015-4-7	174	44	44	43	43
2016-2-26	97	33	32	32	0

Table 4.1: Selected nights and number of frames in individual filters.

Prior to further analysis, all frames were reduced using the `IRAF` software package (Tody 1986). The reduction process included bias subtraction and flat-field correction, which were performed using the `imarith` task.

The initial analysis was performed using data from a single night, specifically 2014-4-6, which contains the largest number of frames (Tab. 4.1). Variable star detection was carried out using the `ISIS` software package (Alard and Lupton 1998), which is based on the image subtraction method described in Sect. 3.5. The configuration of `ISIS` was optimized for the given dataset. The frame was subdivided into 4×4 regions in order to account for spatial variations of the point spread function. The convolution kernel was modeled using three Gaussian components with widths of $\sigma = 0.7$, 2.0 and 4 pixels. Each component

was modified by a polynomial of degree 6, 4 and 3. Spatial variations of the kernel were described using a first-degree polynomial, while the differential background was assumed to be constant.

The selection of the reference frame represented an important step in the image subtraction process. Prior to the `ISIS` analysis, all frames were visually inspected in order to identify the sharpest frame with the best seeing conditions. Several of these candidate frames were subsequently tested as reference frames in `ISIS`. The final selection was based primarily on the quality of the resulting image subtraction and the clarity of the obtained light curves. The selected reference frame used for the final analysis is shown in Fig. 4.1.

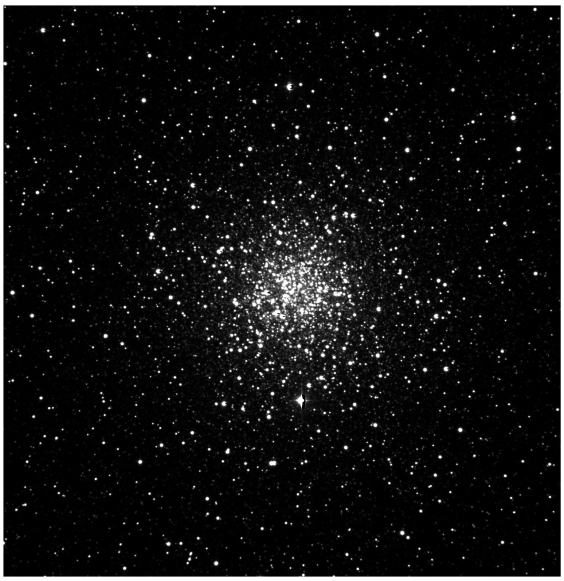

Figure 4.1: Reference frame used for image subtraction analysis in `ISIS`.

The application of the image subtraction method resulted in the detection of several hundred candidate objects. These candidates were further examined using visual inspection of the subtracted frames. In addition, an animation of the subtracted frames was used to identify genuine variable star candidates. True variable objects are expected to appear as circular features, without any apparent structure, that alternate between bright and dark residuals over time, reflecting changes in brightness. Examples of such behavior are shown in Fig. 4.2.

For the selected candidates, light curves were constructed using the photometric measurements provided by `ISIS`. The inspection of light curves was essential for distinguishing real variable stars from false detections caused by noise or image defects. Examples of a variable star and an artefact are shown in Fig. 4.3.

Subsequently, light curves for each of the identified variable stars were analyzed in four photometric filters (B, V, R, I, see Sect. 3.1). The same procedure was then repeated for additional nights. The analysis in multiple filters was performed in order to verify whether the same variable stars could be identified consistently in different filters and to compare the quality of the resulting light curves. This made it possible to find out that the R filter gives the least scattered and best quality light curves. This is demonstrated in Fig. 4.4, where light curves in all four filters are presented, with the R-band curve showing

the clearest variability patterns. Based on this result, only data obtained in the *R* filter were used for further analysis and identification of variable stars. The `ISIS` software was then applied to all selected *R*-band frames from the 11 nights, resulting in a set of light curves for all detected variable stars. The final dataset used for the variability analysis covered a time span from February 2013 to February 2016 (total time span of 1099 days) and consisted of 343 *R*-band frames obtained during 11 observing nights.

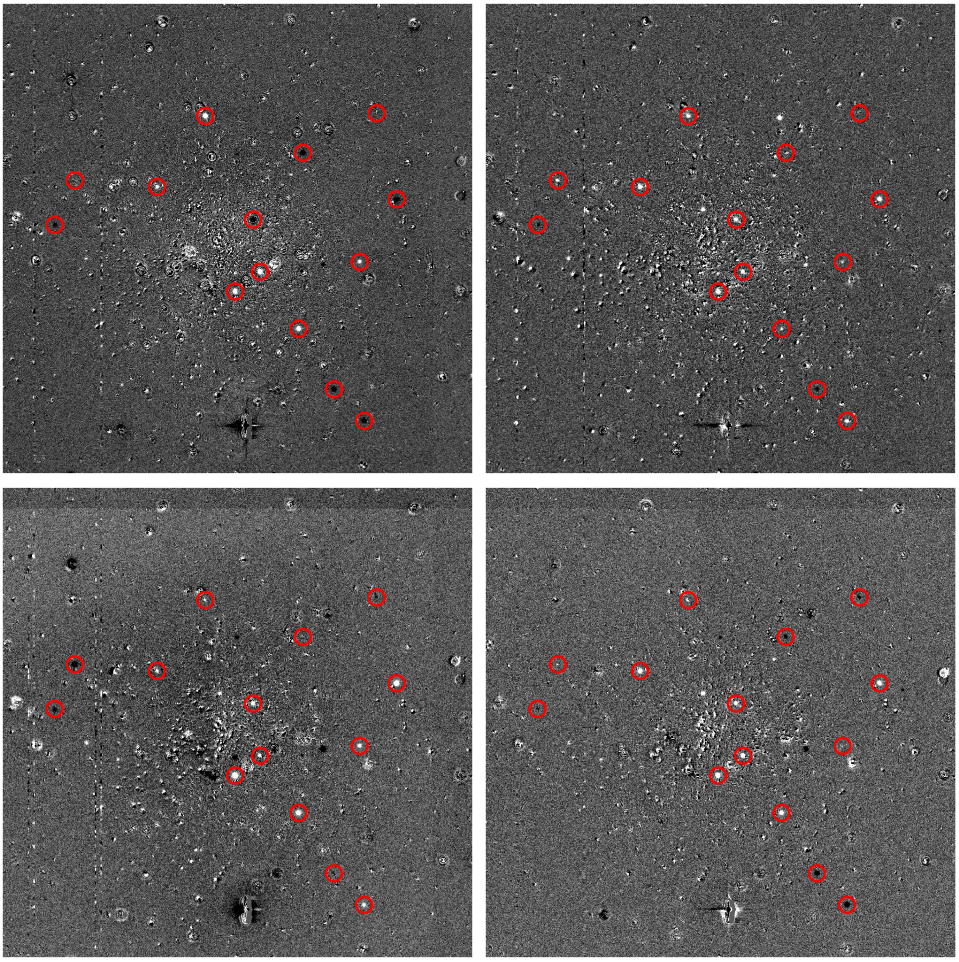

Figure 4.2: Variable stars candidates in subtracted frames.

The `ISIS` software provides measurements in flux units obtained via aperture photometry (Sect. 3.3) applied to the subtracted frames. To convert these measurements into magnitudes, profile photometry (Sect. 3.4) was performed in `IRAF` on the reference frame used in `ISIS`. This provided reference flux and corresponding magnitudes for individual stars. Using Pogson's Eq. (3.3), the flux obtained from `ISIS` was transformed into magnitudes, allowing the construction of light curves in magnitude units.

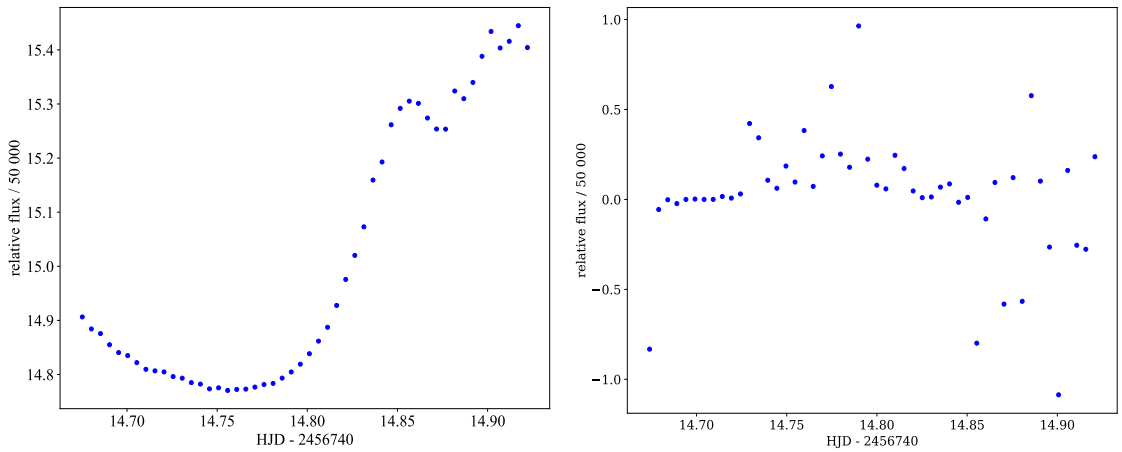

(a) Variable star. (b) Artefact.

Figure 4.3: Example of variable star light curve and a false detection.

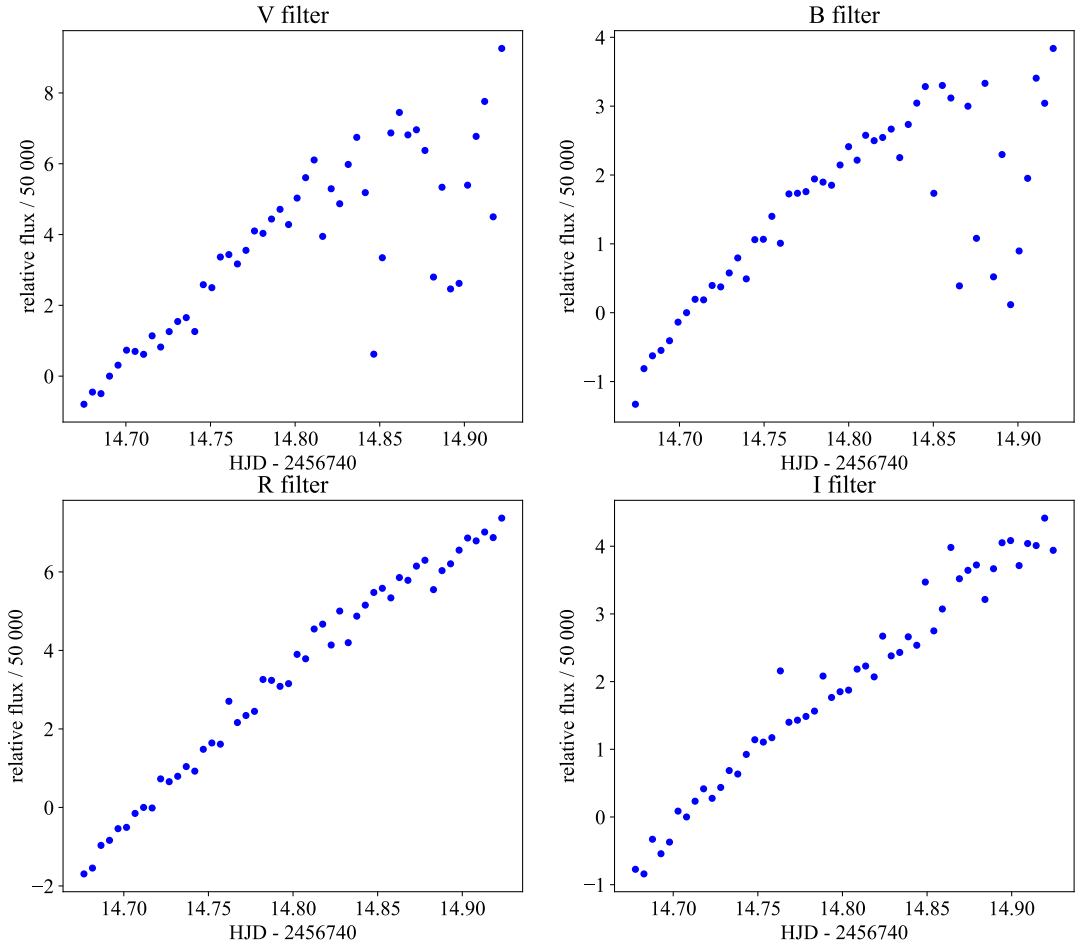

Figure 4.4: Comparison of light curves in four photometric filters.

Chapter 5

Analysis and results

A total of 23 candidate variable stars were identified in the field of the globular cluster NGC 4833. Each object was assigned an identifier from v1 to v23. The candidates and their coordinates are listed in Tab. 5.1, while their positions within the observed field are shown in Fig. 5.1.

Star	RA	DEC	star	RA	DEC
v1	12:59:04.50	-70:52:55.76	v13	12:59:47.03	-70:53:58.54
v2	12:59:07.89	-70:53:33.47	v14	12:59:50.65	-70:52:24.02
v3	12:59:10.01	-70:52:27.25	v15	12:59:52.69	-70:50:39.20
v4	12:59:22.03	-70:53:28.67	v16	12:59:56.94	-70:52:26.91
v5	12:59:23.11	-70:53:30.02	v17	12:59:57.90	-70:50:12.78
v6	12:59:30.20	-70:54:28.84	v18	12:59:59.66	-70:54:32.34
v7	12:59:32.91	-70:53:10.11	v19	13:00:03.21	-70:53:19.96
v8	12:59:35.60	-70:52:01.05	v20	13:00:26.78	-70:49:18.21
v9	12:59:35.56	-70:52:16.46	v21	13:00:31.77	-70:52:57.69
v10	12:59:39.85	-70:52:17.93	v22	13:00:44.86	-70:47:28.24
v11	12:59:45.96	-70:54:28.02	v23	12:59:38.59	-70:53:01.88
v12	12:59:46.55	-70:51:29.99			

Table 5.1: Variable stars in NGC4833.

The initial analysis was performed using observation from the night 2014-4-6, which contains the largest number of images. Light curves obtained during the night are shown in Fig. 5.2. These data were important for the identification of variability types, since the relatively dense sampling allowed characteristic shapes of several light curves to be recognized directly from the observations.

For further analysis, periods of variability were determined for most objects using the `Period04` software (Lenz and Breger 2005). Based on the derived periods, the light curves were phase-folded, and the final phased light curves were produced (Fig. 5.3). However, the total amount of available observational data was limited, which significantly affected the

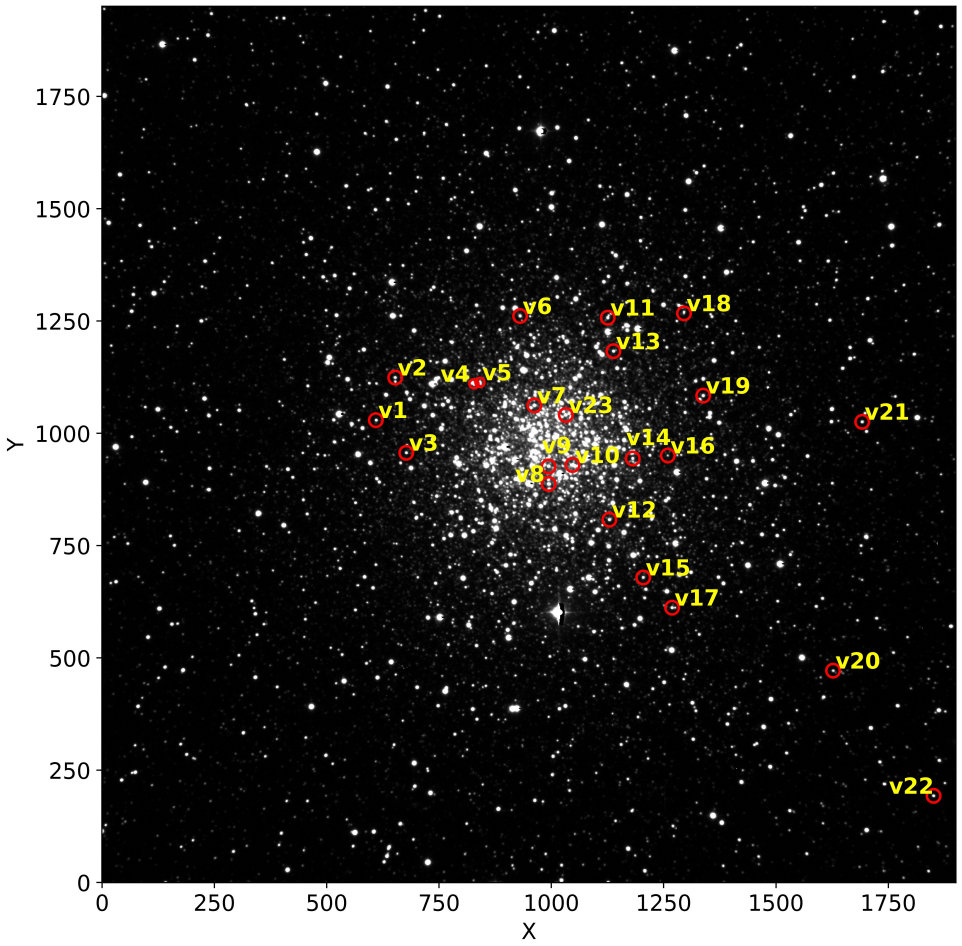

Figure 5.1: Variable stars in NGC 4833.

quality of some phase-folded light curves. In several cases, the phase coverage is incomplete and the determination of periods remains uncertain. An example of a frequency spectrum obtained using `Period04` is shown in Fig. 5.4. In addition to the dominant frequency peak, several nearby alias peaks are visible.

For this reason, the classification of variable stars was based not only on the phased light curves, but also on the shapes of the original light curves obtained during the best-sampled observing night. The detected frequencies, periods and preliminary classifications of the identified variable stars are summarized in Tab. 5.2.

The majority of the detected variable stars were classified as RR Lyrae candidates. These candidates exhibit periods ranging from approximately 0.35 to 0.85 days, corresponding to frequencies between about 1.1 and 2.7 c/d. In some cases, alias frequencies are possible but the contained periods remain consistent with the expected range for RR Lyrae variables described in Sect. 1.4.1.

Their light curves show characteristic behavior with relatively large amplitudes and asymmetric shapes, consisting of a steep rise in brightness followed by a slower decline. Several objects, including v2, v4, v8, v10, v13, v14, v17 and v19, display phased light curves typical of RR Lyrae stars. Objects v5 and v9 may represent either RR Lyrae or

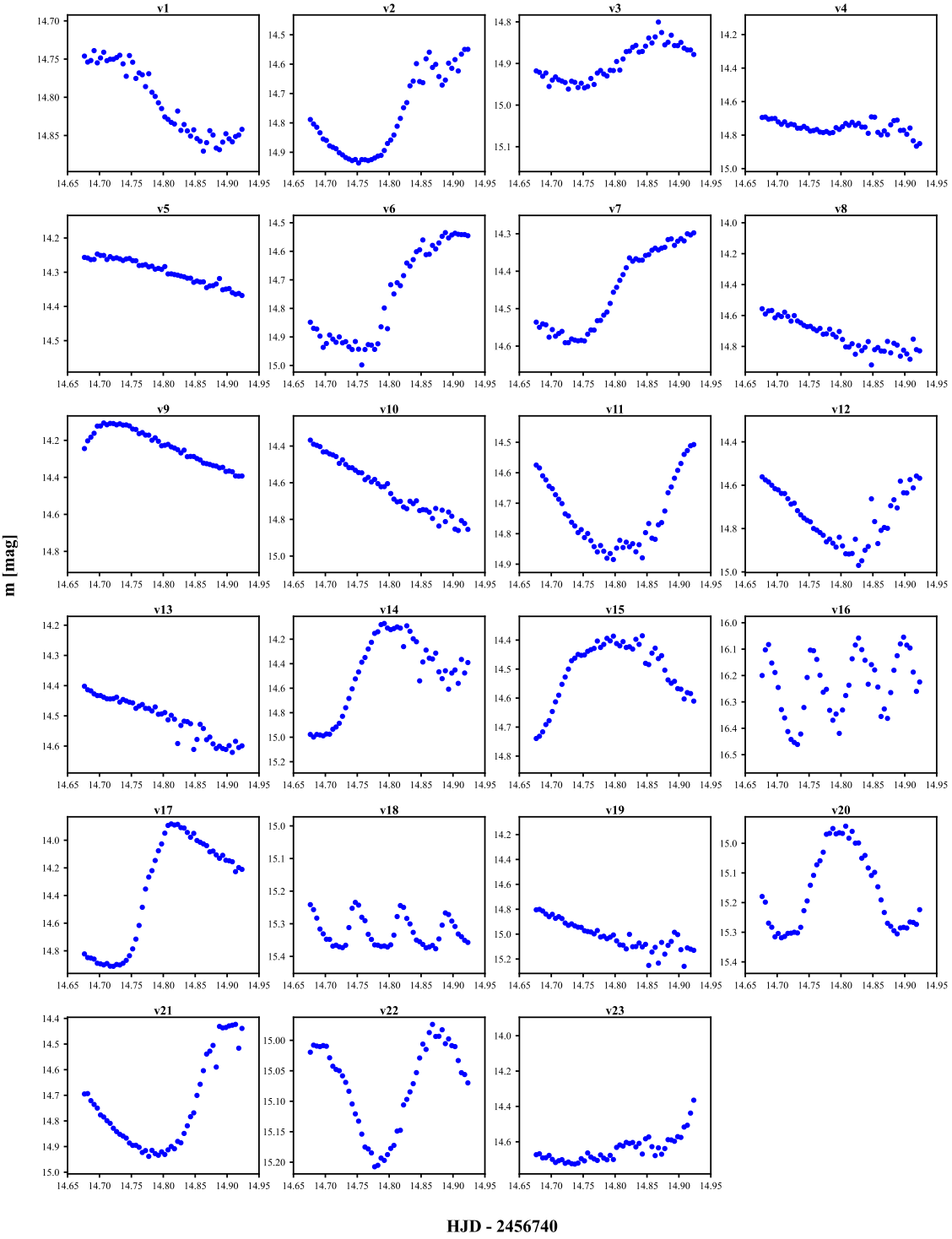

Figure 5.2: Unphased light curves obtained during the night 6.4.2014.

short-period Cepheid candidates. Their longer periods and the shapes of their light curves do not allow an exact classification based solely on the available photometric data in one filter.

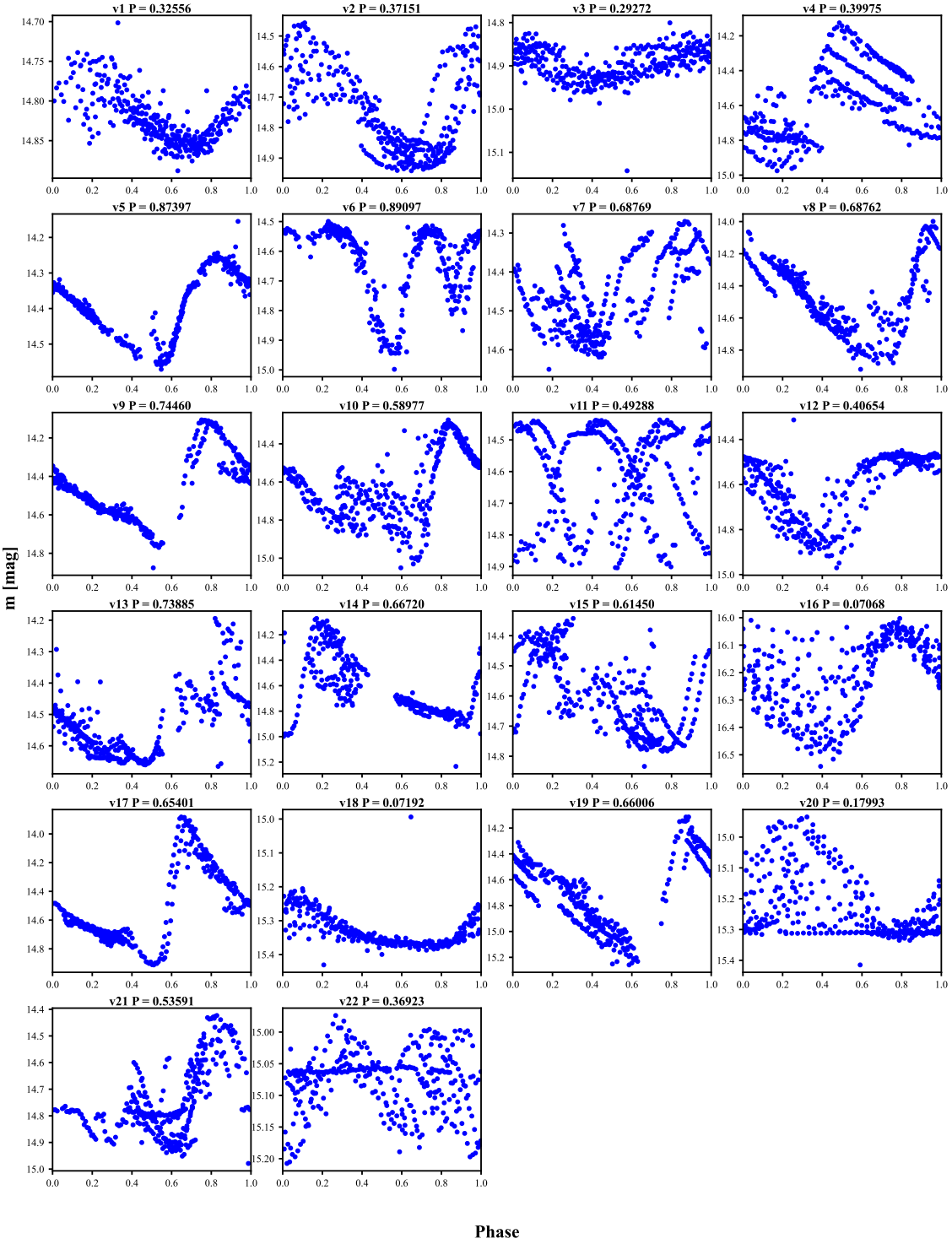

Figure 5.3: Phase-folded light curves using the determined variability periods.

Two objects, v16 and v18, were classified as SX Phoenicis candidates. These stars exhibit significantly higher frequencies $f_{\mathrm{v16}} = 14.1486$ c/d and $f_{\mathrm{v18}} = 13.9049$ c/d, corresponding to short pulsation periods $P_{\mathrm{v16}} = 0.0707$ days and $P_{\mathrm{v18}} = 0.0719$ days. Their short periods and relatively rapid brightness variations are characteristic of SX Phoenicis stars

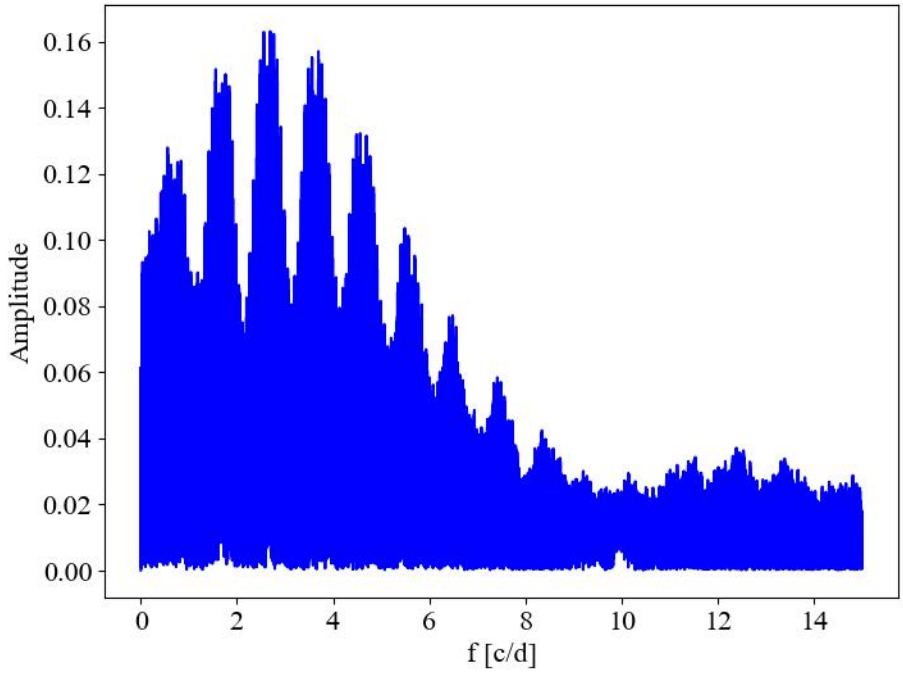

Figure 5.4: Example of frequency spectrum for variable star v2.

mentioned in Sect. 1.4.1. The phased and also unphased light curves of v16 and v18 show relatively coherent periodic behavior, despite the limited observational data, supporting their classification as SX Phoenicis. Several objects were classified as possible eclipsing binaries or rotational variables. In particular, v1 and v3 exhibit frequencies near 3 c/d, corresponding to a period of about 0.3 days. Their light curves may correspond either to rotational modulation or binary variability. Additional observation would be required to distinguish between these two types of variability.

Objects v6 and v22 were classified as binary candidates due to the shape of their light curves being typical of binary system variables mentioned in Sect. 1.3.2. They have periods of approximately 0.9 and 0.4 days, although in the case of v6, an alternative alias frequency is possible.

The classification of some objects remains uncertain due to an insufficient amount of observational data. In particular, v20 and v23 do not exhibit clearly recognizable phased light curves and may represent artefacts caused by image defects or noise. For object v23, no reliable period could be determined. Consequently, this object could not be phase-folded and its variability remains uncertain.

Star	f [c/d]	P [d]	Type
v1	3.07161	0.32556	Rot/Bin
v2	2.69175	0.37150	RR Lyr
v3	3.41622	0.29272	Rot/Bin
v4	2.50154	0.39975	RR Lyr
v5	1.14420	0.87397	RR Lyr/Ceph
v6	1.12237	0.89097	Bin
v7	1.45414	0.68769	RR Lyr
v8	1.45430	0.68762	RR Lyr
v9	1.34300	0.74460	RR Lyr/Ceph
v10	1.69557	0.58977	RR Lyr
v11	2.02890	0.49288	RR Lyr
v12	2.45976	0.40654	RR Lyr/Bin
v13	1.35345	0.73886	RR Lyr
v14	1.49880	0.66720	RR Lyr
v15	1.62735	0.61450	RR Lyr
v16	14.14858	0.07068	SX Phe
v17	1.52904	0.65401	RR Lyr
v18	13.90486	0.07192	SX Phe
v19	1.51501	0.66006	RR Lyr
v20	5.55779	0.17993	Var
v21	1.86600	0.53591	RR Lyr
v22	2.70833	0.36923	Bin
v23	-	-	Var

Table 5.2: Variable stars in NGC 4833 with their frequencies, periods and variable type.

Discussion and conclusions

In this thesis, photometric observations of the globular cluster NGC 4833 obtained with the 1.54 m telescope at La Silla observatory were analyzed. The data were reduced using the `IRAF` software package, while the detection of variable stars was performed using the image subtraction method implemented in `ISIS`.

The analysis of photometric data resulted in the identification of 23 candidate variable stars listed in Tab. 5.1. Light curves were constructed for all objects and their variability periods were analyzed using the `Period04` software package.

Most of the detected objects exhibit properties consistent with RR Lyrae stars described in Sect. 1.4.1. In addition, several candidates for eclipsing binaries, rotational variables and SX Phoenicis were identified. All of the detected candidate variable stars with their periods, frequency and variable type are listed in Tab. 5.2.

The classification of variable stars was based primarily on the shape of their light curves, derived periods, and comparison with the characteristic properties of known variability types discussed in Chapter 1. However, the reliability of the classification is limited by the relatively small amount of available observational data. Although images from 11 nights were used, the temporal coverage remains insufficient for some objects, which complicates accurate period determination. The limited sampling of the observations resulted in the presence of strong alias frequencies in the periodograms of all stars.

For this reason, the classification was not based solely on phase-folded light curves. The original unphased light curves obtained during the observing night with the largest number of images (6.4.2014) were also considered. The relatively dense sampling during this night allowed several variability patterns to be recognized directly from the observational data, even in cases where the phased light curves remain ambiguous.

Two objects, v16 and v18, were classified as likely SX Phoenicis candidates due to their short pulsating periods. Since SX Phoenicis stars are commonly associated with blue straggler stars in globular clusters (see Sect. 1.4.1), these objects may represent particularly interesting targets for future observations.

Several objects, especially v20 and v23, may represent artefacts rather than genuine variable stars. Their phased light curves do not show clear periodic behavior and the derived frequencies are uncertain or absent. The classification of these objects remains uncertain. Image defects, noise or insufficient photometric precision may have contributed to these detections.

An additional objective of this thesis was to investigate whether any of the detected variable stars could be associated with chemically peculiar star candidates identified in Špoková et al. (2026). No clear correspondence between the detected variable stars and the published chemically peculiar stars was found. Moreover, no variability was detected by

the ISIS software at the position of the chemically peculiar stars reported in the literature. However, variability in chemically peculiar stars is often characterized by amplitudes of only a few hundredths of a magnitude, which is below the photometric precision and quality of the obtained light curves. Therefore, low-amplitude variability of these objects cannot be excluded and may simply remain undetected in the available data.

Overall, the image subtraction method combined with the profile photometry was successfully applied to the analysis of the observational data in this work, confirming its suitability for detecting variable stars in crowded stellar fields such as globular clusters. Additional observations with better temporal coverage would be necessary to improve period determination and confirm the proposed classification of several objects. Further improvement could also be achieved through more detailed selection of the observational data, for example by excluding nights affected by poorer observational conditions and subsequently repeating the period analysis. In addition, future analysis could include the remaining observing nights from the original set of 32 nights, which were not used in the present work. A larger data set could improve the phase coverage of the light curves and reduce the influence of alias frequencies. Additional analysis of the data obtained in other photometric filters could provide further information about the detected variables. Future work may also include the construction of HR diagrams. Despite the limitations of the available data, the obtained results contribute to the study of variable stars in NGC 4833 and may serve as a basis for future observations.

Bibliography

Alard, C. and Robert H. Lupton (1998). "A Method for Optimal Image Subtraction". In: *The Astrophysical Journal* 503.1, pp. 325–331. DOI: 10.1086/305984.

Arellano Ferro, A. and Z. Prudil (2026). "Distance and [Fe/H] of Galactic bulge clusters from member RR Lyrae I-band light curves". In: *Monthly Notices of the Royal Astronomical Society* 548.1, stag586. DOI: 10.1093/mnras/stag586.

Arkelyan, N. R. and S. V. Pilipenko (2022). "Globular Cluster as Indicators of Galactic Evolution". In: *Astronomy Reports* 66.3, pp. 191–199. DOI: 10.1134/S10637729220300\-15.

Bognár, Zsófia and Ádám Sódor (2025). "Selected Results on Variable Stars Observed by TESS". In: *Universe* 11.9, p. 319. DOI: 10.3390/universe11090319. URL: https://www.mdpi.com/2218-1997/11/9/319.

Boyles, J. et al. (2011). "Young Radio Pulsars in Galactic Globular Clusters". In: *The Astrophysical Journal* 742.1, p. 51. DOI: 10.1088/0004-637X/742/1/51.

Carretta, E. et al. (2014). "The extreme chemistry of multiple stellar populations in the metal-poor globular cluster NGC 4833". In: *Astronomy & Astrophysics* 564, A60. DOI: 10.1051/0004-6361/201323321.

Carretta, Eugenio (2021). "Potassium abundances in multiple stellar populations of the globular cluster NGC 4833". In: *Astronomy & Astrophysics* 649, A154. DOI: 10.1051/0004-6361/202140684.

Chahal, Deepak et al. (2022). "Statistics of BY Draconis chromospheric variable stars". In: *Monthly Notices of the Royal Astronomical Society* 514.4, pp. 4932–4943. DOI: 10.1093/mnras/stac1660.

Chomiuk, Laura, Brian D. Metzger, and Ken J. Shen (2021). "New Insights into Classical Novae". In: *Annual Review of Astronomy and Astrophysics* 59.1, pp. 391–444. DOI: 10.1146/annurev-astro-112420-114502.

Cousins, A. W. J. (1976). "VRI standards in the E regions". In: *Memoirs of the Royal Astronomical Society* 81, p. 25.

Eggen, Joe (2008). *A Report on the Theory of Pulsating Stars*. Accessed: 2026-05-10. URL: https://www.astro.gsu.edu/~wiita/pulsating_stars2.pdf.

European Southern Observatory (ESO) (2008). *ESO Image eso0844a*. Image credit: ESO, License: CC BY 4.0. URL: https://www.eso.org/public/images/eso0844a/.

Fernie, John Donald, Eric J. Chaisson, and Helen Sawyer Hogg-Priestly (2025). *Star cluster*. Encyclopaedia Britannica, Accessed: 2026-04-25. URL: https://www.britanni%5C-ca.com/science/star-cluster.

Forbes, Duncan A. and Terry Bridges (2010). "Accreted versus in situ Milky Way globular clusters". In: *Monthly Notices of the Royal Astronomical Society*. DOI: 10.1111/j.1365-2966.2010.16373.x.

Gratton, Raffaele et al. (2019). "What is a globular cluster? An observational perspective". In: *The Astronomy and Astrophysics Review* 27.1. DOI: 10.1007/s00159-019-0119-3.

Janík, Jan (2021). *Astronomické pozorováníe*. Masarykova univerzita, Přírodovědecká fakulta. URL: https://astro.physics.muni.cz/download/documents/skrip%5C-ta/F4200.pdf.

Johnson, H. L. and W. W. Morgan (1953). "Fundamental stellar photometry for standards of spectral type". In: *The Astrophysical Journal* 117, p. 313. DOI: 10.1086/145697.

Kopal, Zdenek (1955). "The classification of close binary systems". In: *Annales d'Astrophysique* 18, p. 379.

Kron, G. E. and J. L. Smith (1951). "Red and infrared magnitudes for 125 stars in ten areas". In: *The Astrophysical Journal* 113, p. 324. DOI: 10.1086/145403.

Lenz, Patrik and Michel Breger (2005). "Period04 User Guide". In: *Communications in Asteroseismology* 146, pp. 53–136. DOI: 10.1553/cia146s53.

Liu, Shi-Qi et al. (2026). "The Phenomenological Classification of TESS Eclipsing Binaries". In: *arXiv e-prints*. eprint: 2604.26398.

Mereghetti, Sandro (2013). "Pulsars and Magnetars". In: *Brazilian Journal of Physics* 43.5–6, pp. 356–368. DOI: 10.1007/s13538-013-0137-y.

Mikulášek, Zdeněk and Miloslav Zejda (2013). *Proměnné hvězdy*. Masarykova univerzita, Přírodovědecká fakulta. URL: https://astro.physics.muni.cz/download/documents/skripta/F5540.pdf.

OGLE Project (2011a). *OGLE Atlas of Variable Star Light Curves: Classical Cepheids*. Accessed: 2026-04-30. URL: https://www.astrouw.edu.pl/~soszynsk/atlas/classical_Cepheids.html.

— (2011b). *OGLE Atlas of Variable Star Light Curves: RR Lyrae Stars*. Accessed: 2026-04-30. URL: https://www.astrouw.edu.pl/~soszynsk/atlas/RR_Lyr.html.

Percy, John R. (2007a). "Pulsating variable stars". In: *Understanding Variable Stars*. Cambridge: Cambridge University Press, pp. 136–223.

— (2007b). *Understanding Variable Stars*. Cambridge: Cambridge University Press.

Pogson, Norman (1856). "Magnitudes of Thirty-six of the Minor Planets". In: *Monthly Notices of the Royal Astronomical Society* 17, pp. 12–15. DOI: 10.1093/mnras/17.1.12.

Pych, W. et al. (2001). "Cluster AgeS Experiment. CCD photometry of SX Phoenicis variables in the globular cluster M 55". In: *Astronomy & Astrophysics* 367, pp. 148–158. DOI: 10.1051/0004-6361:20000349.

Schöller, Markus and Swetlana Hubrig (2015). "Magnetic chemically peculiar stars". In: *arXiv e-prints*. DOI: 10.48550/arXiv.1501.04225. eprint: 1501.04225.

Shafter, A. W. et al. (2021). "A Survey of Novae in M83". In: *The Astrophysical Journal* 923.2, p. 239. DOI: 10.3847/1538-4357/ac2c79. eprint: 2110.00676.

Špoková, M. et al. (2026). "Chemically peculiar candidates in 18 Milky Way Globular Clusters". In: *Astronomy & Astrophysics*. in press. DOI: 10.1051/0004-6361/202558329. URL: https://www.aanda.org/articles/aa/pdf/forth/aa58329-25.pdf.

Stetson, Peter B. (1987). "DAOPHOT: A Computer Program for Crowded-Field Stellar Photometry". In: *Publications of the Astronomical Society of the Pacific* 99, p. 191. DOI: 10.1086/131977.

Tody, Doug (1986). "The IRAF Data Reduction and Analysis System". In: *Instrumentation in Astronomy VI*. Vol. 627, p. 733. DOI: 10.1117/12.968154.

VandenBerg, Don A. et al. (2013). "The ages of 55 globular clusters as determined using an improved method". In: *The Astrophysical Journal* 775.2, p. 134.